Pore Structure Characterization of Porous Silica by 1H NMR Using Water, Benzene, and Cyclohexane as Probe Molecules

ARTICLE *in* THE JOURNAL OF PHYSICAL CHEMISTRY · JULY 1996

Impact Factor: 2.78 · DOI: 10.1021/jp960305t

3 AUTHORS, INCLUDING:

Eddy Walther. Hansen
University of Oslo
112 PUBLICATIONS **1,459** CITATIONS

SEE PROFILE

Pore Structure Characterization of Porous Silica by ^{1}H NMR Using Water, Benzene, and Cyclohexane as Probe Molecules

Eddy Walther Hansen,* Ralf Schmidt, and Michael Stöcker

SINTEF Applied Chemistry, P.O. Box 124, Blindern, N-0314 Oslo, Norway

Received: January 31, 1996[⊗]

The pore size distribution of four commercial silica materials saturated with water have been derived from experimental ^{1}H NMR intensity vs temperature curves (*IT*-curves) of the confined water. The observed melting points or transition temperatures of benzene and cyclohexane confined in the same materials are shown to be consistent with corresponding data obtained from the water *IT*-curves. In general, the freezing point depression (ΔT) of these fluids can be related to the pore radius R in accordance with a modified Gibbs−Thompson equation: $\Delta T = K/(R + d)$, where K and d are constants characteristic of the confined fluid. The melting point depressions of benzene and cyclohexane are shown to be more sensitive to pore radius than that of water; i.e., the two former have a larger K-value. Moreover, the average pore radius of these materials can be estimated from ^{1}H NMR chemical shift measurements of the benzene-saturated samples. Simulation of ^{1}H NMR spectra of benzene confined in mixtures of silica (mesopores) and zeolite (micropores) will be presented.

Introduction

To our knowledge, Pearson et al.[1] and Resing et al.[2,3] were the first to report on ^{1} H NMR temperature measurements of water confined in porous materials some 20 and 30 years ago. During the last few years, this same NMR approach has been adopted by Strange et al.,[4−5] Overloop et al.,[6] and Hansen and co-workers[7−11] to derive pore size distributions of porous materials. Strange et al. used primarily cyclohexane as a probe molecule, while the two latter groups used water as a probe molecule in order to derive pore size distributions. The theoretical basis for this NMR application is the well-known Gibbs−Thompson equation[12,13] which relates the freezing point depression (ΔT) of a confined liquid to the pore radius (R), according to: $\Delta T = T_0 - T = (2\gamma T_0/R\rho\Delta H)$, where T_0 is the normal bulk melting point, T is the melting point of the confined solid of dimension R, γ is the surface tension, ρ is the density of the solid, and ΔH is the enthalpy of fusion. Assuming all parameters in the Gibbs−Thompson equation to be independent of temperature and pore dimension, this equation will take the very simple form $\Delta T = K/R$, where the constant K is characteristic of the absorbent. Measurement of the proton NMR signal intensity (I) vs temperature (T), denoted as an *IT*-curve, thus enables the pore size distribution (dI/dR) to be determined from the derivative of the *IT*-curve, i.e., $dI/dR = -(K/R^2)(dI/dT)$.

Hansen and co-workers[7,8] derived a mathematical formula relating the NMR intensity to the inverse of the absolute temperature under certain conditions and showed that the derivative of the NMR signal intensity with respect to $1/T$ ($dI/d(1/T)$) could be expressed by a sum of Gaussian functions containing $1/T$ as a variable. They were thus able to determine the distribution of melting temperatures and pore size distribution curves from a direct model fit to the observed *IT*-curve. In this work, the pore size distribution of four water-saturated commercial mesoporous silica materials, derived from experimental *IT*-curves, will be presented. Corresponding melting points or transition temperatures of benzene and cyclohexane confined in these same materials will be discussed with reference to the *IT*-curves of the water-saturated samples. In particular, we will comment on the advantage and limitations in using benzene or cyclohexane as probe molecules. Moreover, we will show that the observed average proton chemical shift of benzene confined in these materials can provide a simple way of estimating the average pore dimension of the materials.

Experimental Section

The four silica materials investigated in this work were commercial Kiselgel 40, 60, 100, and 200 from Merck with nominal pore diameters of 40, 60, 100, and 200 Å, respectively. In the following discussion these materials will be denoted as A, B, C, and D, respectively. All samples were dried completely for 2 days or more at a temperature of 403 K in a conventional oven. The probe molecules (water, benzene, cyclohexane) were then added to each sample under an inert atmosphere of N_2. All samples were overfilled with fluid (≈150%). One of the samples (B) was characterized by N_2 adsorption in order to check the consistency in pore size determined by NMR and N_2 adsorption. The water-saturated samples were studied by ^{1}H NMR at subzero temperature ($T < 273$ K) using a Varian Gemini NMR spectrometer, operating at 300 MHz proton resonance frequency. The accuracy of the temperature determination was ±0.5 K. A bandwidth of 50 kHz, an acquisition time of 0.10 s, and a 90° pulse of 16 μs were applied with a repetition time of 15 s between the rf-pulses. Each spectrum was composed of four transients. The long interpulse timing was dictated by the long spin−lattice relaxation time of potential silanol protons, which exhibit spin−lattice relaxation times of approximately 3 s.[6,7] The free induction decay was sampled after blanking the receiver for 20 μs, thus enabling the signal from the solid ice phase to be ignored because of its very short spin−spin relaxation rate in the range of a few microseconds. Moreover, due to the extremely long spin−lattice relaxation time (T_1) of the water protons of solid ice at this high magnetic field strength ($T_1 \approx 900$ s at 263 K and 7.05 T),[14,15] any residual signal from the solid ice phase would be significantly reduced when taking into account the pulse repetition time of 15 s used in this work. The temperature was changed in steps of 1 K, if

* To whom correspondence should be addressed.

[⊗] Abstract published in *Advance ACS Abstracts,* June 1, 1996.

S0022-3654(96)00305-X CCC: $12.00

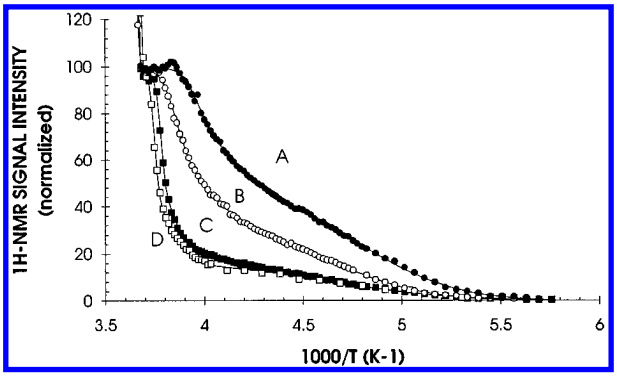

Figure 1. ^{1}H NMR signal intensity vs temperature (*IT*-curve) of water confined in samples A−D. Solid lines represent nonlinear least-squares fit to eq 1.

not otherwise stated in the text. A temperature equilibration of 2 min was applied before any measurement was initiated. The intensities were determined by numerical integration of the peaks and were corrected for temperature according to Curie's law,[16] i.e., the NMR signal intensity measured at a temperature T was corrected by multiplication by the factor T/T_0, with $T_0 =$ 273.15 K. The inherent uncertainty in determining the area of an NMR peak is approximately 1−5%. The ^{1}H NMR *IT*-curve was obtained by slowly cooling the sample to 173 K and then heating the sample to 280 K while recording the different NMR spectra.

The ^{1}H NMR spectra of the benzene-saturated samples were monitored under the same conditions, except for a somewhat longer receiver blanking time of 50 μs. A rather different approach was chosen in the case of cyclohexane. When using the simple single-pulse technique, as just outlined, a significant amount of residual signal from cyclohexane was detectable far below the normal freezing point of bulk cyclohexane at 279.5 K. As proposed by Strange et al.,[4,5] the frozen and the liquid components of this probe molecule are better distinguished on the basis of T_2. We thus adopted this idea and applied a simple Carr−Purcell pulse sequence with a waiting time τ between the $\pi/2$-pulse and the second π-pulse. The interpulse timing (τ) was chosen so that the NMR signal of "solid" bulk cyclohexane was just unobservable below its normal melting point; i.e., τ was determined to be 0.5 ms.

Results and Discussion

Melting of Water, Benzene, and Cyclohexane Confined in Porous Silica. Figure 1 shows the observed *IT*-curves of the four water-saturated silica materials A, B, C, and D. The solid lines represent model fits (eq 1)[7,8] to the observed data

$$I(X) = \sum_{i=1}^{N} \frac{I_{0i}}{\sqrt{\pi}} \int_0^{(X-X_{ci})/(\sqrt{2}\Delta_i)} \exp(-u^2)\, du \qquad (1)$$

where I_{0i}, X_{ci}, and Δ_i represent the intensity, the inverse transition temperature ($X_{ci} = 1000/T_{ci}$), and the width of the temperature distribution curve of phase i, respectively. X (=1000/T) represents the inverse absolute temperature. The parameter u is just an integration variable. The fitted parameters are shown in Table 1. As can be seen from the analytical form of eq 1, the temperature distribution curve (dI/dX) is a simple sum of Gaussian functions centered at X_{ci} with half-width Δ_i. These temperature distribution curves are shown in Figure 2 and represent unique fingerprints of the porous materials. In order

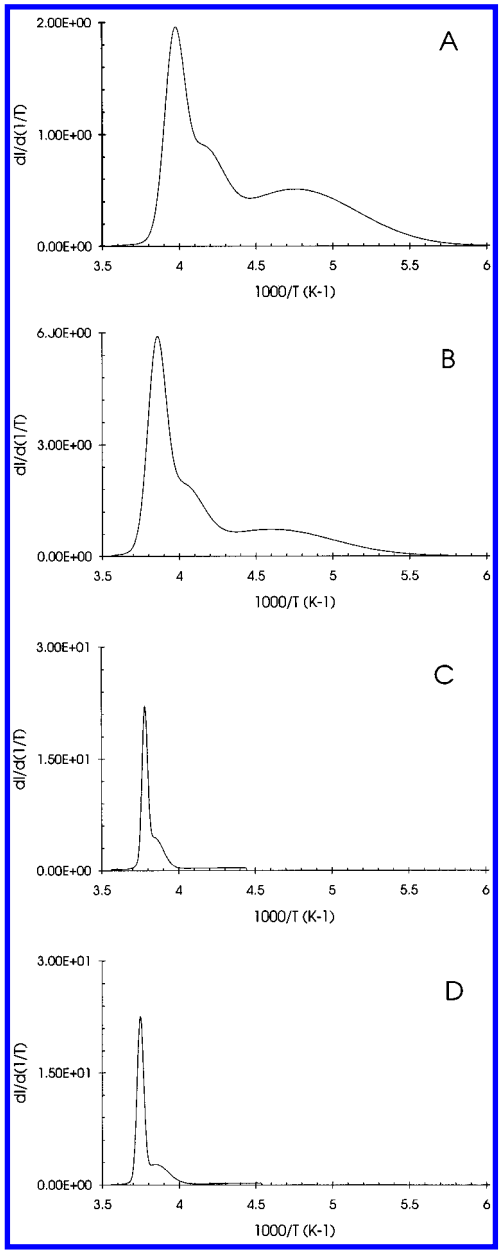

Figure 2. Normalized melting point distribution curves, dI/d(1/T), of water confined in samples A−D derived from eq 1.

to determine the actual pore size distribution, eq 2 was used[8]

$$\frac{dI}{dR} = \sum_{i=1}^{N} \frac{I_{0i}}{10^3 K\sqrt{2\pi}\Delta_i} (XT_0 - 10^3)^2 \exp\left[-\left(\frac{X - X_{ci}}{\sqrt{2}\Delta_i}\right)^2\right] \qquad (2)$$

However, when applying eq 2 the constant K, which is identical to the parameter found in the Gibbs−Thompson equation

$$\Delta T = K\frac{1}{R} \qquad (3a)$$

must be determined. Previous investigations on well-characterized water-saturated mesoporous MCM-41 materials, having particularly narrow pore size distributions, have shown that eq 3a must be somewhat modified,[8] i.e.

$$\Delta T = \frac{K}{R - d} \qquad (3b)$$

with $K = K_w = (515 \pm 19.6)$ K Å and $d = d_w = (3.06 \pm$

TABLE 1: Numerical Values of the Parameters X_{ci} (= 1000/T_{ci}), I_{0i} and Δ_i (See Eq 1) and Pore Radius R (Eqs 2 and 4a)

sample	i	water X_{ci} (K^{-1})	water I_{0i}	water Δ_i (K)	water R (Å)	benzene X_{ci} (K^{-1})	cyclohexane X_{ci} (K^{-1})
A	1	3.660				3.590	3.574
	2	3.969 ± 0.017	26 ± 21	0.064 ± 0.023	28.5	4.391 ± 0.023	3.834 ± 0.018
	3	4.152 ± 0.143	23 ± 11	0.129 ± 0.097	20.3		4.826 ± 0.019
	4	4.756 ± 0.068	51 ± 6	0.404 ± 0.045	12.8	5.282 ± 0.059	
					18.4[a]		
B	1	3.657				3.596	3.574
	2	3.855 ± 0.004	36 ± 13	0.058 ± 0.010	44.5	4.146 ± 0.018	3.967 ± 0.006
	3	4.021 ± 0.073	27 ± 15	0.129 ± 0.047	27.7		4.554 ± 0.087
	4	4.601 ± 0.059	37 ± 4	0.399 ± 0.039	14.7	5.190 ± 0.161	
					29.0[a]		
C	1	3.661				3.592	3.561
	2	3.781 ± 0.002	43 ± 7	0.018 ± 0.003	63.7	3.771 ± 0.003	3.806 ± 0.003
	3	3.843 ± 0.017	29 ± 8	0.056 ± 0.010	47.4	3.897 ± 0.058	3.818 ± 0.010
	4	4.342 ± 0.121	28 ± 4	0.605 ± 0.081	20.2	4.451 ± 0.420	
					47.0[a]		
D	1	3.664				3.594	
	2	3.749 ± 0.003	56 ± 11	0.021 ± 0.005	87.9	3.706 ± 0.005	
	3	3.848 ± 0.047	27 ± 14	0.081 ± 0.038	49.0	3.974 ± 0.051	
	4	4.620 ± 0.333	17 ± 7	0.503 ± 0.310	15.5		
					64.1[a]		

[a] Average pore radius determined by numerical integration of eq 4a. See text for further details.

0.36) Å. A suffix "w" has been introduced in order to differentiate the *K*-values and the *d*-values derived for water, benzene, and cyclohexane, respectively. Our previously reported interpretation of this equation is that water molecules confined within pores of radius R do not actually see or sense a pore restriction R, but rather sense an effective pore of smaller dimension, equal to $R - d_w$, which is explained as the existence of a surface layer of mobile water molecules one or two molecular layers thick (d_w), acting as an interface shield between the solid matrix and the inner solid ice core. We will later in this work present an alternative physical explanation for the apparent deviation of the experimental data (eq 3b) from the Gibbs−Thompson relation (eq 3a). The pore size distributions of the four silica materials, as determined from eq 2, are depicted in Figure 3 and reveal distributions composed of three well-defined peak maxima. The abrupt and sharp transition observed at the highest temperature (smallest *X*-value) in the *IT*-curve represents the melting point of bulk water and serves as a useful temperature calibration point. This transition point is thus not included in the derived pore size distributions shown in Figure 3. A better resolution than 1 K in the *IT*-curve is not possible on our instrument and suggests that the largest pore that can be determined when using water as a probe molecule is $R \approx 500$ Å. In practice, pore sizes larger than $R \approx 200$ Å are difficult to determine accurately. When comparing the average NMR pore size ($R = 29.0$ Å) of sample B (Figure 3) with the corresponding average pore size derived using N_2 adsorption, ($R = 26-30$ Å), a good agreement is found. However, as can be seen from Figure 3B, a much better resolution is obtained with NMR compared to the latter technique. Whether the improved resolution obtained by NMR is significant or not remains to be answered. Anyhow, the experimental proton NMR results reveal three significantly different transition temperatures, which is confirmed by replica measurements on three identical samples.

The term "average" needs some explanation, since this term is used throughout in this work. The general definition of an average pore size ($\bar{R}$), derived from a pore size distribution function, dI/dR, is

$$\bar{R} = \frac{\int_{R_{min}}^{R_{max}} R \frac{dI}{dR}\, dR}{\int_{R_{min}}^{R_{max}} \frac{dI}{dR}\, dR} \qquad (4a)$$

By insertion of eqs 2 and 3b into eq 4a, the average value of the pore radius can be determined by an integral involving the inverse temperature X (=1000/T) rather than R. This integral is solved numerically, and the results are summarized in Table 1.

The *IT*-curves of benzene and cyclohexane confined in the same silica materials are shown in Figure 4a,b. Only three of the samples containing cyclohexane were investigated. The narrow and abrupt transition observed at high temperature (T_0) corresponds to the melting of bulk solid and agrees well with tabulated values of $T_{0benzene} = 278.5$ K ($X_{0benzene} = 3.591$ K^{-1}) and $T_{0cyclohexane} = 279.5$ K ($X_{0cyclohexane} = 3.578$ K^{-1}), respectively. In the case of sample D, the benzene-saturated sample did not reveal any low-temperature transition as found in the corresponding water-saturated sample. Since the relative intensity contribution of water to this low-temperature phase transition was estimated to be approximately 17%, a corresponding low-temperature transition would be expected when substituting water with benzene as a probe molecule. However, keeping in mind the large relative uncertainty of ±7%, the true intensity contribution might be less than 10% and may explain why this temperature transition is not observed in the benzene-saturated sample D. Moreover, benzene confined in samples A and B revealed only a single "high"-temperature transition, in contrast to the water saturated samples which revealed two distinct "high"-temperature transitions. The reason for this is most probably caused by the poorer resolution (due to less number of points) in the *IT*-curve of benzene in this temperature range. In order to compare the two observed high-temperature transitions of the water-saturated samples (X_{c2}, X_{c3}) with the observed single temperature transition of the benzene-saturated samples, an average "high" transition temperature ($\bar{X}$) of the two water samples was estimated by eq 4b

$$\bar{X} = \frac{I_2 X_{c2} + I_3 X_{c3}}{I_2 + I_3} \qquad (4b)$$

which represents a weighted average of the two transition temperatures. I_i ($i = 2, 3$) is the intensity contribution to phase i (Table 1). The results are shown in Figure 5 where the melting point depressions (ΔT_b) of benzene are plotted vs the melting point depressions (ΔT_w) of water for all the samples. It is reasonable to assume that the melting point depression of benzene confined in the porous materials follows the same pore

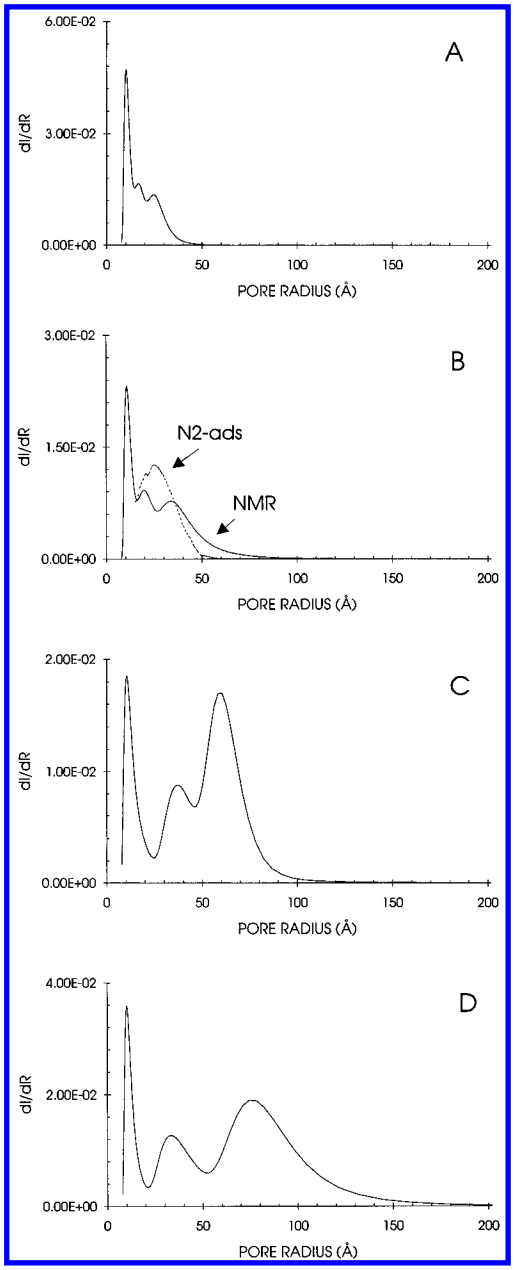

Figure 3. Pore size distribution curves, d*I*/d*R*, of samples A−D derived from eq 2. The dotted line in B represents the pore size distribution derived from N_2 adsorption measurements.

size dependence as given by eq 3b with K and d replaced by K_b and d_b, respectively. From the combination of these equations, i.e., eliminating the pore radius R, the following equation is derived

$$\Delta T_b = K_b \frac{\Delta T_b}{K_w + (d_b - d_w)\Delta T_w} \qquad (5)$$

The solid line in Figure 5A shows a nonlinear least-squares fit of eq 5 to the observed data points with $K_b = (1107 \pm 86)$ K Å and $d_b = (6.97 \pm 1.09)$ Å.

A corresponding analysis of the cyclohexane-saturated samples is shown in Figure 5B and gives $K_c = (867 \pm 164)$ K Å and $d_c = -(1.36 \pm 2.58)$ Å. Within experimental error these results suggest that benzene and cyclohexane are approximately twice as sensitive (K_b, $K_c \approx 2K_w$) for mapping out the pore structure compared to water as a probe molecule; i.e., benzene can be used to determine pore sizes up to $R \approx 1000$ Å, or in practice

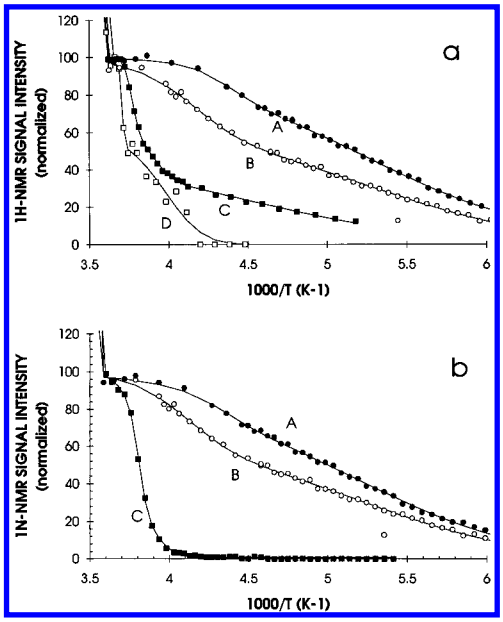

Figure 4. ^{1}H NMR signal intensity vs temperature (*IT*-curve) of benzene (a) and cyclohexane (b) confined in samples A−D. Solid lines represent nonlinear least-squares fit to eq 1.

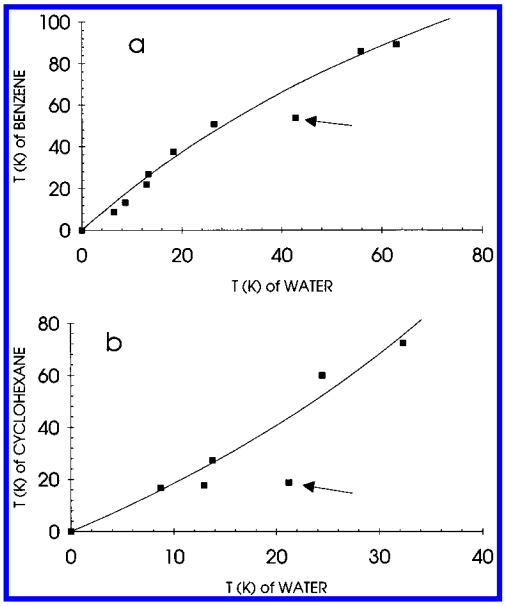

Figure 5. Melting point depression of benzene (a) and cyclohexane (b) vs melting point depression of water confined in samples A−D. Solid lines represent model fits (eq 5). Points marked with an arrow are omitted in the model fit.

pore sizes up to approximately $R \approx 500$ Å. However, water seems to be a better probe molecule for characterizing small pores.

Strange et al.[4,5] have reported a sensitivity of cyclohexane of approximately three times larger than for water, which is a 50% higher sensitivity than that reported in this work. We believe the reason for this discrepancy to be related to the difference in magnetic field strengths. In the former case a proton NMR frequency of 21.5 MHz was used, while in the present work a 300 MHz proton frequency was applied. Differences in magnetic field strength might influence T_2 and, in particular, the magnetic susceptibility difference between matrix and fluid. Another important point is that T_2 at this high magnetic field strength might change with temperature and pore dimension, which has not been reported at low magnetic field.[4,5] If T_2 is changing with temperature/pore dimension, the spin-echo technique, with fixed interpulse timing (τ) between the

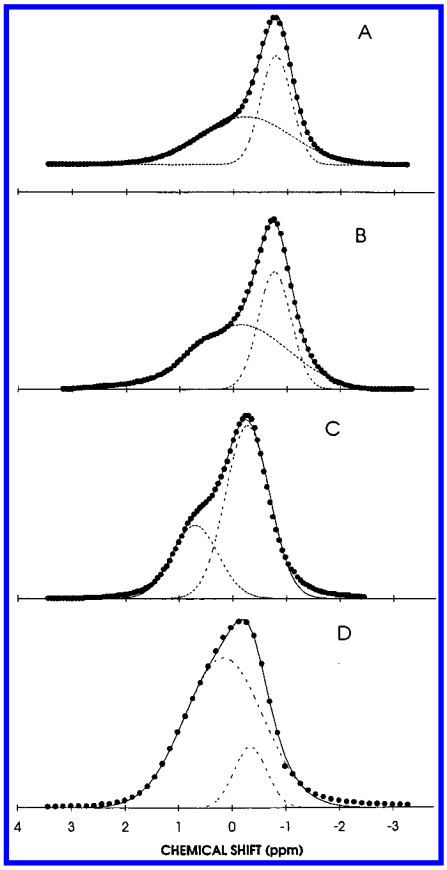

Figure 6. ^{1}H NMR spectra of benzene confined in samples A−D. Dotted lines represent nonlinear least-squares fit of two Gaussian functions to the observed spectrum. The solid lines represent the overall fit.

first $\pi/2$-pulse and the second π-pulse, might give erroneous relative intensities at two different temperatures or pore radii. Further investigation of this phenomenon is required.

Within experimental error, the d-values determined for the three fluids are in agreement with the existence of a liquid-like, mobile surface layer of thickness d. However, eq 3b might be reformulated to give

$$\Delta T = K\frac{R}{R-d}\frac{1}{R} \tag{6}$$

suggesting that the factor $(2\gamma T_0)/(\rho\Delta H)$ in the Gibbs−Thompson equation is equal to $KR/(R-d)$ and thus is not a constant but is dependent on the pore dimension R. This way of rearranging eq 3b leads to an alternative physical interpretation which is supported by measurements performed by Jackson et al.[17] who found that the molar heat of fusion of a number of organic liquids confined in controlled pore glasses decreased with decreasing pore dimension. This observation is in agreement with eq 6, which predicts a reduction in the molar heat of fusion with decreasing pore radius R, for $R > d > 0$, if the density and surface tension are independent of R. Also, a negative value of d would be acceptable within the concept of this model, suggesting that the molar heat of fusion would increase with decreasing pore radius.

Chemical Shift of Benzene Confined in Silica Materials. Figure 6 shows the ^{1}H NMR spectra of benzene confined in the silica materials A−D at 277 K, which is 1.5 K below the normal melting point of benzene. The chemical shift was measured relative to the chemical shift of bulk benzene at room temperature. The reason for performing the measurements at this temperature is to assure that the interparticle liquid benzene

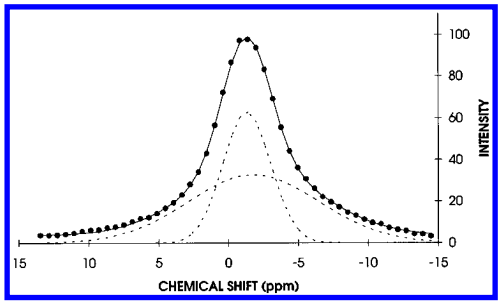

Figure 7. ^{1}H NMR spectra of benzene confined in sample E (Y-zeolite). Dotted lines represent nonlinear least-squares fit of two Gaussian functions to the observed spectrum. The solid lines represent the overall fit.

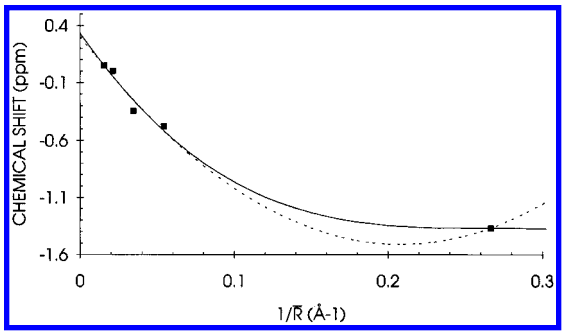

Figure 8. Average chemical shift of benzene vs inverse average pore size of samples A−D. The curves represent model fits to eq 7b based on spherical (—) and cylindrical (- - -) pore geometry. See text for further details.

is frozen out and does not affect the NMR spectrum. The shapes of the spectra are neither purely Gaussian nor purely Lorentzian but contain shoulders which suggest that the chemical shift might be dependent on the actual pore size distribution of the silica materials. We have fitted the NMR spectra to a sum of two Gaussian functions (Gaussian functions gave a better fit than Lorentzian functions) as indicated on Figure 6. However, we were not able to find any correlation between the derived chemical shifts and the pore sizes tabulated in Table 1. It is worth noting that using statistical validity tests an optimal fit to the observed NMR spectra was obtained by a sum of four Gaussian functions (not shown). Moreover, the average chemical shift of the spectrum was calculated using eq 4a with dI/dR replaced by the NMR absorption spectrum, $I(\delta)$, and R replaced by the chemical shift δ. Also, a commercial Y-zeolite (sample E, Ventron GMBH) with pore dimension $R = 3.7$ Å has been analyzed by the same procedure. In this case only two Gaussian functions were needed to fit the observed spectrum (Figure 7). Figure 8 shows a plot of the average chemical shift ($\bar{\delta}$) vs the inverse average pore radius ($1/\bar{R}$). Assuming the benzene molecules in the "interior" of the pore to behave like bulk benzene in fast exchange with benzene molecules at the interface (thickness d), between the solid matrix and the interior of the pore, the average chemical shift of benzene within the porous material can be estimated

$$\bar{\delta} = \frac{V_s}{V_T}\delta_s + \frac{V_b}{V_T}\delta_b \tag{7a}$$

where V_T is the total pore volume, V_s is the volume of the surface layer of thickness d, and V_b is the residual pore volume, i.e., $V_b = V_T - V_s$. δ_b and δ_s are the chemical shifts of bulk benzene and benzene at the surface, respectively. Depending on pore geometry, eq 7a can be written

$$\bar{\delta} = \delta_s + (\delta_b - \delta_s)\left(1 - \frac{d}{R}\right)^n \qquad (7b)$$

where $n = 2$ for cylindrical pores (dotted line in Figure 8) and $n = 3$ for spherical pores (solid line in Figure 8). Fitting eq 7b to the observed data points in Figure 8 gives $\delta_s = -(1.51 \pm 0.14)$ ppm, $\delta_b = -(0.30 \pm 0.11)$ ppm, and $d = (4.80 \pm 0.44)$ Å for cylindrical pore geometry and $\delta_s = -(1.37 \pm 0.08)$ ppm, $\delta_b = -(0.33 \pm 0.11)$ ppm, and $d = (3.80 \pm 0.70)$ Å for spherical pores, respectively. The minimum in the chemical shift vs $1/\bar{R}$ observed for the cylindrical pore model has—to our knowledge—no physical explanation and might originate from the simplifications and assumptions used in deriving eqs 7a and 7b. It is reasonable to expect that the assumption of a two-phase model in fast exchange breaks down when $\bar{R}$ approaches d. We can therefore not make any definite conclusion from these results whether or not the pore structure is spherical or cylindrical. It is worth noting that the d-value determined by chemical shift measurements has the same order of magnitude as the d-value determined from NMR *IT*-measurements, $d = (6.97 \pm 1.09)$ Å. In fact, within a 95% confidence interval, the two methods predict the same value of d.

From the data presented in Figure 8, the chemical shift decreases markedly with decreasing pore dimension down to about $\bar{R} = 10$ Å. Below this pore radius, the chemical shift decreases only slightly. This observation suggests that the spectrum of benzene confined in a porous material containing both micropores ($R < 10$ Å) and mesopores (10 Å $< R <$ 250 Å) might give rise to a resolved spectrum amenable for quantitative separation of mesopores and micropores. To test this hypothesis, a sample was prepared by mixing a Y-zeolite (sample E) and a mesoporous silica (sample D) in pore volume ratio of approximately 3:7. The ^{1}H NMR spectrum is shown in Figure 9. In the following discussion the normalized NMR spectra of the two individual samples will be denoted $D(\delta)$ and $E(\delta)$, respectively, where δ is the chemical shift. The NMR spectrum of a mechanical mixture of the two samples can then be written

$$M(\delta) = A_d[pE(\delta) + (1 - p)D(\delta)] \qquad (8)$$

where p represents the fraction of zeolite and A_d is an adjustable parameter representing the total area of the spectrum. This equation has been fitted to the observed spectrum of the sample mixture (thick, solid line in Figure 9) with $p = 0.28 \pm 0.03$. The same equation has been applied to simulate the NMR spectra of samples containing different relative amounts of D and E, as displayed in Figure 9, with $p = 0.1$, 0.2, 0.3, 0.6, and 1, respectively. A_d was chosen so that the amplitude of the spectra was the same.

The observed spectrum fits the simulated spectrum rather well and indicates that the amount of micropores within a porous material can be estimated from the proton NMR spectrum of benzene confined in such materials. These results are only preliminary. Measurements on different types of well-characterized porous materials are necessary to confirm this more general hypotheses.

Conclusion

The pore size distribution curves of four commercial silica materials have been derived from experimental ^{1}H NMR intensity vs temperature curves (*IT*-curves) of water confined in these materials at subzero temperature. Corresponding *IT*-curves of cyclohexane and benzene confined in the same mesoporous materials are shown to be consistent with the melting point curves derived from the corresponding water-saturated samples. In general, the freezing point depression (ΔT) of these fluids can be related to the pore radius R, according to the Gibbs−Thompson equation: $\Delta T = K(R/(R - d))(1/R)$, where K and d are constants characteristic of the confined fluid. Two different physical concepts have been discussed to rationalize this equation. The freezing point depressions of benzene and cyclohexane are shown to be more sensitive to pore radius than that of water; i.e., the two former have a larger K-value. The average pore radii of these materials are shown to be related to the average ^{1}H NMR chemical shift of confined benzene in these materials, suggesting that the relative amount of mesopores and micropores can be determined from a simple NMR spectral analysis.

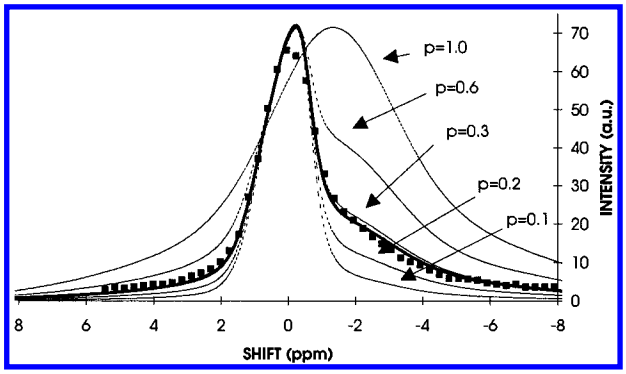

Figure 9. ^{1}H NMR spectrum of benzene (■) confined in a powder mixture of samples D and E. The thick, solid line represents model fit (eq 8) to the spectrum. The other curves in the figure represent simulated spectra based on eq 8 with $p = 0.1$, 0.2, 0.3, 0.6, 1.0, respectively. $p = 1.0$ represents the spectrum of pure sample E (Y-zeolite). See text for further details.

References and Notes

(1) Pearson, R. T.; Derbyshire, W. *J. Colloid Interface Sci.* **1974**, *46*, 232−248.
(2) Resing, H. A.; Thompson, J. K; Krebs, J. J. *J. Phys. Chem.* **1964**, *7*, 1621.
(3) Resing, H. A. *J. Phys. Chem.* **1965**, *43*, 669.
(4) Strange, J. H.; Rahman, M.; Smith, E. G. *Phys. Rev. Lett.* **1993**, *71*, 3589−3591.
(5) Alnami, S. M.; Strange, J. H.; Smith, E. G. *Magn. Reson. Imaging* **1994**, *12*, 257−259.
(6) Overloop, K.; Van Gerven, L. *J. Magn. Reson., Ser. A* **1993**, *101*, 179.
(7) Hansen, E. W.; Schmidt, R.; Stöcker, M.; Akporiaye, D. *J. Phys. Chem.* **1995**, *99*, 4148−4154.
(8) Schmidt, R.; Hansen, E. W.; Stöcker, M.; Akporiaye, D; Ellestad, O. H. *J. Am. Chem. Soc.* **1995**, *117*, 4049−4056.
(9) Schmidt, R.; Stöcker, M.; Hansen, E. W.; Akporiaye, D.; Ellestad, O. H. *Microporous Mater.* **1995**, *3*, 443−448.
(10) Akporiaye, D.; Hansen, E. W.; Schmidt, R.; Stöcker, M. *J. Phys. Chem.* **1993**, *97*, 7743.
(11) Hansen, E. W.; Stöcker, M.; Schmidt, R. *J. Phys. Chem.*, in press.
(12) Gibbs, J. W. T*he Collected Works of J. Williard Gibbs*; Academic Press: New York, 1928).
(13) Thompson, W. (Lord Kelvin) *Philos. Mag.* **1871**, *42*, 448−452.
(14) Barnaal, D. E.; Lowe, I. J. *J. Chem. Phys.* **1967**, *48*, 4614.
(15) Barnaal, D. E.; Kopp, M.; Lowe, I. J. *J. Chem. Phys.* **1976**, *65*, 5495.
(16) Abragam, A. *The Principles of Nuclear Magnetism*; Clarendon Press: Oxford, U.K., 1961.
(17) Jackson, C. L.; McKenna, G. B. *J. Chem. Phys.* **1990**, *93*, 9002−9011.

JP960305T